ANNALS of Clinical and Translational Neurology
Open Access
ANA American Neurological Association since 1875

RESEARCH ARTICLE

Selected missense mutations impair frataxin processing in Friedreich ataxia

Elisia Clark[1,2], Jill S. Butler[3], Charles J. Isaacs[2], Marek Napierala[3] & David R. Lynch[1,2]

[1]University of Pennsylvania, Philadelphia, Pennsylvania
[2]Children's Hospital of Philadelphia, Philadelphia, Pennsylvania
[3]University of Alabama at Birmingham, Birmingham, Alabama

Correspondence
David R. Lynch, Division of Neurology, The Children's Hospital of Philadelphia, 502 Abramson Research Center, 3615 Civic Center Blvd, Philadelphia, PA 19104-4318. Tel: 215-590-2242; Fax: 215-590-3779; E-mail: lynchd@mail.med.upenn.edu

Funding Information
This work was supported in part by the NIH training program in neuropsychopharmacology at the University of Pennsylvania (R01MH109260), as well as by grants from the NIH (R21NS087343) and (R01NS081366 to MN) and the Friedreich Ataxia Research alliance to DRL, MN, and JSB.

Received: 10 March 2017; Revised: 23 May 2017; Accepted: 24 May 2017

Annals of Clinical and Translational Neurology **2017; 4(8): 575–584**

doi: 10.1002/acn3.433

[Correction added on 8 August 2017 after first online publication: the last name of the fourth author was incorrectly spelled and was changed from Napierela to Napierala.]

Abstract

Objective: Frataxin (FXN) is a highly conserved mitochondrial protein. Reduced FXN levels cause Friedreich ataxia, a recessive neurodegenerative disease. Typical patients carry GAA repeat expansions on both alleles, while a subgroup of patients carry a missense mutation on one allele and a GAA repeat expansion on the other. Here, we report that selected disease-related FXN missense mutations impair FXN localization, interaction with mitochondria processing peptidase, and processing. **Methods**: Immunocytochemical studies and subcellular fractionation were performed to study FXN import into the mitochondria and examine the mechanism by which mutations impair FXN processing. Coimmunoprecipitation was performed to study the interaction between FXN and mitochondrial processing peptidase. A proteasome inhibitor was used to model traditional therapeutic strategies. In addition, clinical profiles of subjects with and without point mutations were compared in a large natural history study. **Results**: FXN^{I154F} and FXN^{G130V} missense mutations decrease $FXN^{81–210}$ levels compared with FXN^{WT}, FXN^{R165C}, and FXN^{W155R}, but do not block its association with mitochondria. FXN^{I154F} and FXN^{G130V} also impair FXN maturation and enhance the binding between $FXN^{42–210}$ and mitochondria processing peptidase. Furthermore, blocking proteosomal degradation does not increase $FXN^{81–210}$ levels. Additionally, impaired FXN processing also occurs in fibroblasts from patients with FXN^{G130V}. Finally, clinical data from patients with FXN^{G130V} and FXN^{I154F} mutations demonstrates a lower severity compared with other individuals with Friedreich ataxia. **Interpretation**: These data suggest that the effects on processing associated with FXN^{G130V} and FXN^{I154F} mutations lead to higher levels of partially processed FXN, which may contribute to the milder clinical phenotypes in these patients.

Introduction

Friedreich ataxia (FRDA) affects about one in every 50,000 people in the United States. This slowly progressive ataxia frequently begins in the first decade of life and is associated with dysarthria, spasticity in the lower limbs, scoliosis, absence of lower limb reflexes, and loss of position and vibration sense.[1–3] At present, there is no cure or effective treatment. FRDA is characterized by decreased expression of the mitochondrial FXN protein, from the frataxin gene on chromosome 9. FXN is important for proper mitochondrial function, but the mechanism by which decreased expression leads to disease pathology is not entirely known.[4] FRDA is most commonly caused by an expansion of a GAA repeat tract in the first intron of the *FXN* gene on both alleles, and less commonly by a GAA repeat on one allele accompanied by a point mutation in the other *FXN* allele. In typical FRDA, the length of the shortest GAA expansion correlates with disease severity; longer GAA expansions result in earlier onset and a faster progression.[5–7] The phenotype of patients who carry a GAA expansion on one allele and a missense mutation on the other allele cannot be predicted with certainty; these patients can have a mild or severe clinical outcome,[8] creating a unique platform to understand clinical and genetic heterogeneity. In general, patients carrying

G130V mutations have milder phenotypes in single case reports and small series. In contrast, individuals with mutations in W155R and R165C have much more severe phenotypes.[9–12]

Upon entry into the mitochondria, $FXN^{1–210}$ is processed by mitochondria processing peptidase (MPP) into $FXN^{42–210}$, followed by $FXN^{81–210}$. Many missense mutations in the C-terminus end of FXN have been identified in FRDA, yet, few have been characterized in vivo or in situ. Some are proposed to disrupt mRNA expression (various splice site mutations such as c.165 + 1 G>A and c.384 −2 A>G),[11,12] translation initiation (c.1A>T, c.2T>C, c.2delT, c.3 g>T, c.3G>A), or protein folding (L106S).[9,13–15] These should produce little to no functional protein, and their associated phenotype should be severe in conjunction with a long GAA repeat on the other *FXN* allele. In contrast, R165C, W155R, G130V, and I154F mutations are suspected to produce stable protein. However, R165C and W155R lead to biochemical deficiencies in vitro.[16,17] The mechanism behind the disease-causing features of G130V and I154F is less clear, having been suggested to reflect abnormal maturation or dysfunctional FXN in different models.[9] In the present study, we have ascertained the features of these mutants in mammalian cell systems to understand from a cellular perspective how they might lead to dysfunction in FRDA.

Methods

Site-directed mutagenesis

Each FXN mutant was created using the pcDNA3.1 plasmid with wild-type human FXN containing a C-terminus hemagglutin (HA) tag (Addgene Plasmid #31895) and the Agilent QuikChange XL Site-Directed Mutagenesis Kit.

Transfection and immunostaining

Human embryonic kidney (HEK 293) cells were grown on coverslips and transfected via Lipofectamine 2000 reagent with 4 μg of DNA (2 μg FXN and 2 μg mito-GFP). Twenty-four hours after transfection, cells were fixed with 4% paraformaldehyde followed by treatment with blocking buffer containing 5% normal goat serum, 3% Triton X-100, and 1% BSA. Primary antibody to the HA epitope was added at a 1:100 dilution overnight. Alexa Fluor 568 secondary antibody was added at a dilution of 1:100 and cells were imaged by confocal microscopy.

Subcellular fractionation and western blot

Following transfection of FXN-mutant constructs, HEK 293 cells were lysed with buffer containing: 150 mmol/L sodium chloride, 1 mmol/L EDTA, 100 mmol/L Tris-HCl, 1% Triton X-100, 1% sodium deoxycholate, 0.1% sodium dodecyl sulfate, and protease inhibitor cocktail (Millipore #539134) 1:1000 at pH 7.4 for 1 h and centrifuged at 150*g* to collect whole cell lysates. Whole cell lysates were centrifuged at 100*g* followed by 150*g* to separate the soluble mitochondria fraction from the cytosolic fraction, and 100*g* to collect insoluble mitochondria pellet from soluble mitochondria fraction using a Thermo Scientific Mitochondria Isolation Kit for Mammalian Cells (#89874). The protein concentration of each fraction was determined using a BCA protein assay, and 4 μg of each fraction was loaded on a 12% NuPage gel for electrophoresis, followed by transfer to nitrocellulose membranes. Membranes were blocked with 3% milk for 1 h and incubated with primary HA antibody overnight at 4°C. Membranes were then incubated with secondary HRP-conjugated antibody for 2 h and immunoreactive bands were visualized using luminol-enhanced chemiluminescence (ECL) HPR substrate.

Coimmunoprecipitation and western blot

Twenty-four hours after transfection, cells were lysed with buffer containing: 150 mmol/L sodium chloride, 1 mmol/L EDTA, 100 mmol/L Tris-HCl, 1% Triton X-100, 1% sodium deoxycholate, 0.1% sodium dodecyl sulfate, and protease inhibitor cocktail (Millipore #539134) 1:1000 at pH 7.4 for 1 h. For coimmunoprecipitation, 2 μg of MPP primary antibody was added to 800 μg of total lysate and rocked for 2 h at 4°C. The lysate and antibody solution was then added to washed Protein G Agarose beads overnight, rocking back and forth at 4°C. The following day the beads, lysate, and antibody solution were centrifuged at 14,000*g* and washed five times with IP lysis buffer containing: 150 mmol/L sodium chloride, 1 mmol/L EDTA, 100 mmol/L Tris-HCl, 1% Triton X-100, and 0.5% sodium deoxycholate at pH 7.4. Sample buffer (2X) was added to the beads and heated to 100°C for 5 min. The immunoprecipitated proteins were loaded on a 12% NuPage gel. Normal IgG primary antibody was used as a control as well as anti-FXN primary antibody, followed by Trueblot secondary HRP-conjugated antibody (Rockland #18-8841-31) to detect immunoreactive bands.

MG132 Treatment

Transfected cells were treated with 10 μmol/L of MG132, cell-permeable proteasome inhibitor, for 5 h. Following cell lysis, equal amounts of total cell lysate were loaded on a 12% NuPage gel.

Fibroblast FXN levels by Western Blot

Fibroblast cells from healthy controls and FRDA patients with point mutations were lysed in buffer (0.25 mol/L NaCl, 5 mmol/L EDTA, 50 mmol/L HEPES [pH 7.5], 0.1% NP-40, 0.5 mmol/L DTT) supplemented with 0.1% protease inhibitor cocktail (Sigma Aldrich) and kept on ice for 20 min. The lysates were centrifuged at 20,000*g* for 10 min at 4°C. The clarified supernatants were transferred to fresh tubes and protein concentrations were determined by Bradford assay. A quantity of 75 μg of whole cell lysate were separated by SDS-PAGE and transferred to a PVDF membrane. Immunoblotting was performed with antibodies against FXN (Santa Cruz Biotechnology) and GAPDH (Millipore), and the signals were detected by HRP-mediated chemiluminescence. Densitometry was performed using Image J software (NIH), and the calculated signal ratio of $FXN^{42–210}$ to $FXN^{81–210}$ in each group is plotted. The bars represent the average signal for each group: CTRL= 5 fibroblast lines (n = 13), G130V =3 lines (n = 17), and Typical = 7 lines (n = 8). The asterisk indicates significant differences as determined by Student's t-test ($P < 0.05$).

Quantification and statistical analysis

Image J Software was used to quantify FXN levels on western blots and is represented as mean ± SEM. Two-tailed Student's t-test was used to compare mutants to WT. Significance was set at $P < 0.05$. Image J software was also used to calculate Pearson's correlation coefficient for quantification of colocalization in immunofluorescence images.

Clinical measures

Clinical measure results were derived from a long-standing natural history study from 12 American and Australian sites.[18] In this study, data is collected annually on clinical features of > 900 individuals with FRDA. Data from the baseline cross sectional visits were used in this study including overall medical history and scores on the Friedreich Ataxia Rating Scale (FARS) (a quantified neurological exam); Ataxia Staging scale (a disability score); the Timed 25-Foot Walk (T25FW), scored as the reciprocal (a simple performance test of walking); 9-Hole Peg Test (9HPT), scored as the reciprocal (a simple test of hand function); Contrast Letter Acuity test, the sum of the number of letters read on each of three Sloan charts (a quantitative test of vision); and an Activities of Daily Living (ADL) scale. All these measures capture progressive neurological dysfunction in FRDA. The performance measures were also transformed into Z-scores to create composite scores as reported previously. The Z_2 composite is the sum of the Z-scores from T25FW and 9HPT. The Z_3 composite is the sum of Z-scores from T25FW, 9HPT, and overall vision tests.

Results

Selected FRDA-associated missense mutations decrease $FXN^{81–210}$ levels, but do not impair FXN association with mitochondria

To determine the effects of FRDA-associated missense mutations on FXN import into the mitochondria, FXN variants containing a C-terminal HA tag were cotransfected with mito-GFP in HEK 293 cells. Levels of the $FXN^{81–210}$ form of FXN^{I154F} and FXN^{G130V} are lower as determined by western blot compared to FXN^{WT}, while no detectable exogenous $FXN^{81–210}$ was detected following transfection of FXN^{G137V} and FXN^{L106S} constructs (Fig. 1). Confocal microscopy imaging was used to determine localization of the exogenous FXN proteins. FXN^{R165C} and FXN^{W155R} colocalize with mito-GFP and have FXN immunoreactivity comparable to FXN^{WT} (Fig. 2A). FXN^{I154F}, FXN^{G130V}, and FXN^{G137V} colocalize with mito-GFP but have lower FXN immunoreactivity compared to FXN^{WT} (Fig. 2B). Finally, transfection of FXN^{L106S} leads to no FXN immunoreactivity (Fig. 2C). All expressed mutant proteins colocalize with mito-GFP with a Pearson's correlation coefficient greater than 0.98. While FXN^{R165C} and FXN^{W155R} have increased immunoreactivity compared to FXN^{I154F}, FXN^{G130V}, and FXN^{G137V}, the FXN^{I154F}, FXN^{G130V}, and FXN^{G137V} proteins retain their mitochondrial localization.

Selected FRDA-associated missense mutations impair processing from $FXN^{42–210}$ to $FXN^{81–210}$

To investigate further the decrease in $FXN^{81–210}$ levels of particular FXN-mutant proteins, subcellular fractionation and separation of the soluble mitochondrial fraction and the insoluble mitochondrial pellet was performed. Consistent with immunocytochemistry results, transfection of FXN^{R165C} or FXN^{W155R} leads to $FXN^{81–210}$ levels comparable to levels of FXN^{WT}, while transfection of FXN^{I54F} or FXN^{G130V} produces lower levels of $FXN^{81–210}$ (Fig. 3A and 3B). While FXN^{I154F} or FXN^{G130V} lead to low $FXN^{81–210}$ levels, expression of these mutant proteins leads to an increased level of $FXN^{42–210}$ (Fig. 3A and C), suggesting these FXN variants are not processed readily from $FXN^{42–210}$ to the $FXN^{81–210}$ form. Furthermore, these variants also have increased ratios of insoluble to soluble $FXN^{42–210}$

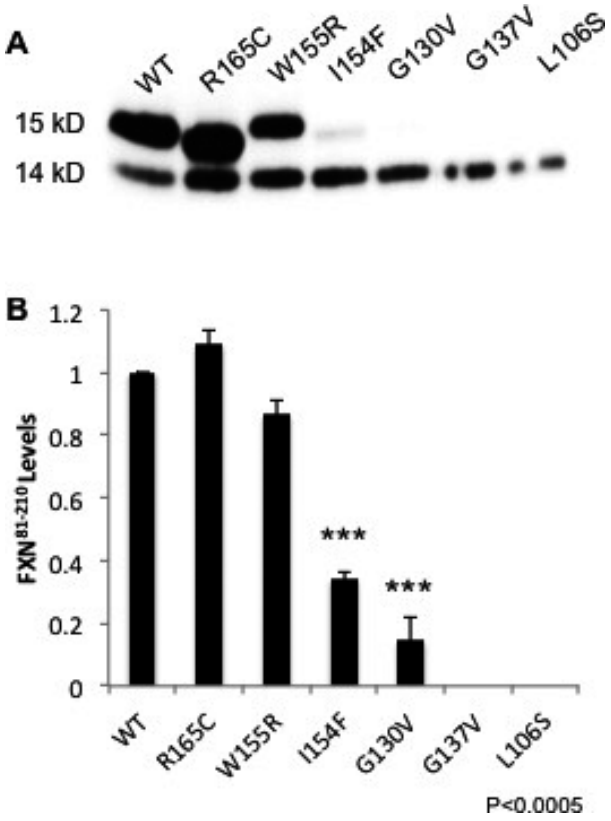

Figure 1. Selected FRDA-associated missense mutations decrease $FXN^{81–210}$ levels. **A.** Western blot of whole cell lysates collected from HEK 293 cells transfected with FXN^{WT}, FXN^{R165C}, FXN^{W155R}, FXN^{I154F}, FXN^{G130V}, FXN^{G137V}, and FXN^{L106S}. An anti-FXN antibody was used to detect both exogenous $FXN^{81–210}$ (15 kD) and endogenous $FXN^{81–210}$ (14 kD) levels after transfection. **B.** Quantification of exogenous FXN levels was normalized to FXN^{WT} and endogenous FXN. Endogenous FXN serves as a loading control. (***) = $P < 0.0005$.

(Fig. 3E-G), suggesting these proteins remain associated with the insoluble inner mitochondrial membrane rather than being released into the soluble portion of the mitochondrion.

Missense mutations FXN^{I154F} and FXN^{G130V} enhance the association of $FXN^{42–210}$ with MPP

To examine the mechanism by which FXN^{I154F} and FXN^{G130V} impair FXN processing, FXN-mutant proteins were coimmunoprecipitated to study the strength of the interaction between FXN and MPP. The $FXN^{42–210}$ forms of FXN^{I154F} and FXN^{G130V} are more readily coimmunoprecipitated by anti-MPP than the $FXN^{42–210}$ form of FXN^{WT}, FXN^{R165C}, and FXN^{W155R} proteins (Fig. 4), suggesting stronger attachment between these variants and MPP.

Increasing FXN^{G130V} and FXN^{I154F} $FXN^{1–210}$ levels does not increase $FXN^{81–210}$ levels

Traditional therapies for FRDA include several strategies designed to increase FXN levels. To model this approach, transfected cells were treated with 10 μmol/L MG132, a proteasome inhibitor, to increase $FXN^{1–210}$ levels in an effort to overcome impaired FXN processing. While FXN^{G130V} and FXN^{I154F} $FXN^{1–210}$ levels increased, as did $FXN^{42–210}$ levels, MG132 treatment did not increase $FXN^{81–210}$ levels (Fig. 5). This suggests that amelioration of these missense mutations cannot be achieved with simple overexpression of precursor FXN, and that there is a true impediment to processing of these mutants to the $FXN^{81–210}$ form.

Impaired FXN processing from $FXN^{42–210}$ to $FXN^{81–210}$ occurs in fibroblasts from FRDA patients with FXN^{G130V}

To analyze the significance of these findings in patient-derived cells and examine the processing of native FXN, western blots were performed on whole cell extracts prepared from control (CTRL) and FRDA G130V patient fibroblasts. Endogenous $FXN^{42–210}$ and $FXN^{81–210}$ FXN levels were detected and expressed as a ratio of $FXN^{42–210}$/$FXN^{81–210}$ (Fig. 6A). The ratio of $FXN^{42–210}$ to $FXN^{81–210}$ is increased in FRDA G130V patient fibroblasts compared to controls ($P < 0.05$). Patient fibroblasts were also immunostained with antibodies to FXN and mitofusin. FRDA G130V patient fibroblasts contain large globular structures (Fig. 6B) consistent with the increased insoluble $FXN^{42–210}$ form detected by western blot and overexpression studies.

FRDA patients with FXN^{G130V} have milder disease features and slower disease progression compared to other heterozygous FRDA patients

We then sought to establish whether patients carrying missense point mutations displayed distinct clinical

Figure 2. Selected FRDA-associated missense mutations do not impair FXN association with mitochondria. Confocal microscopy images of HEK 293 cells cotransfected with mutant FXN constructs and mito-GFP, fixed, and stained using a primary anti-HA antibody to detect exogenous FXN only. Secondary antibodies included Alexa Fluor 568 (FXN) and Alexa Fluor 488 (mito-GFP). DAPI was also used as a nuclear stain. **A.** FXN^{WT}, FXN^{R165C}, and FXN^{W155R}. **B.** FXN^{154F}, FXN^{G130V}, and FXN^{G137V}. **C.** FXN^{L106S}. Pearson's correlation scatter plots of red and green signal intensities for each mutant were generated using Image J Software.

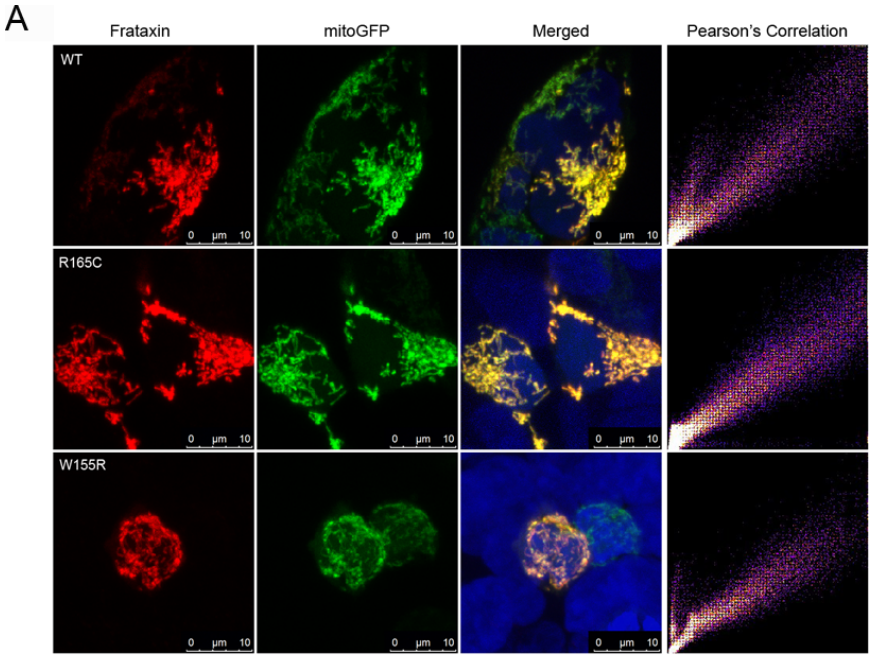

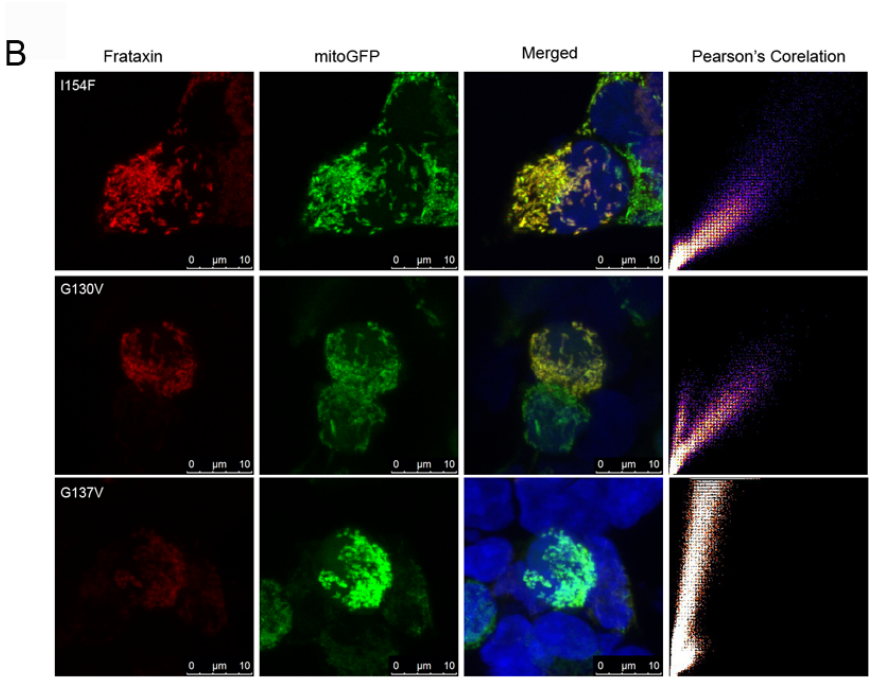

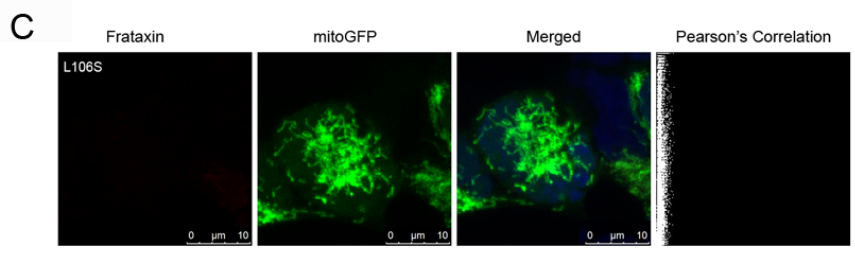

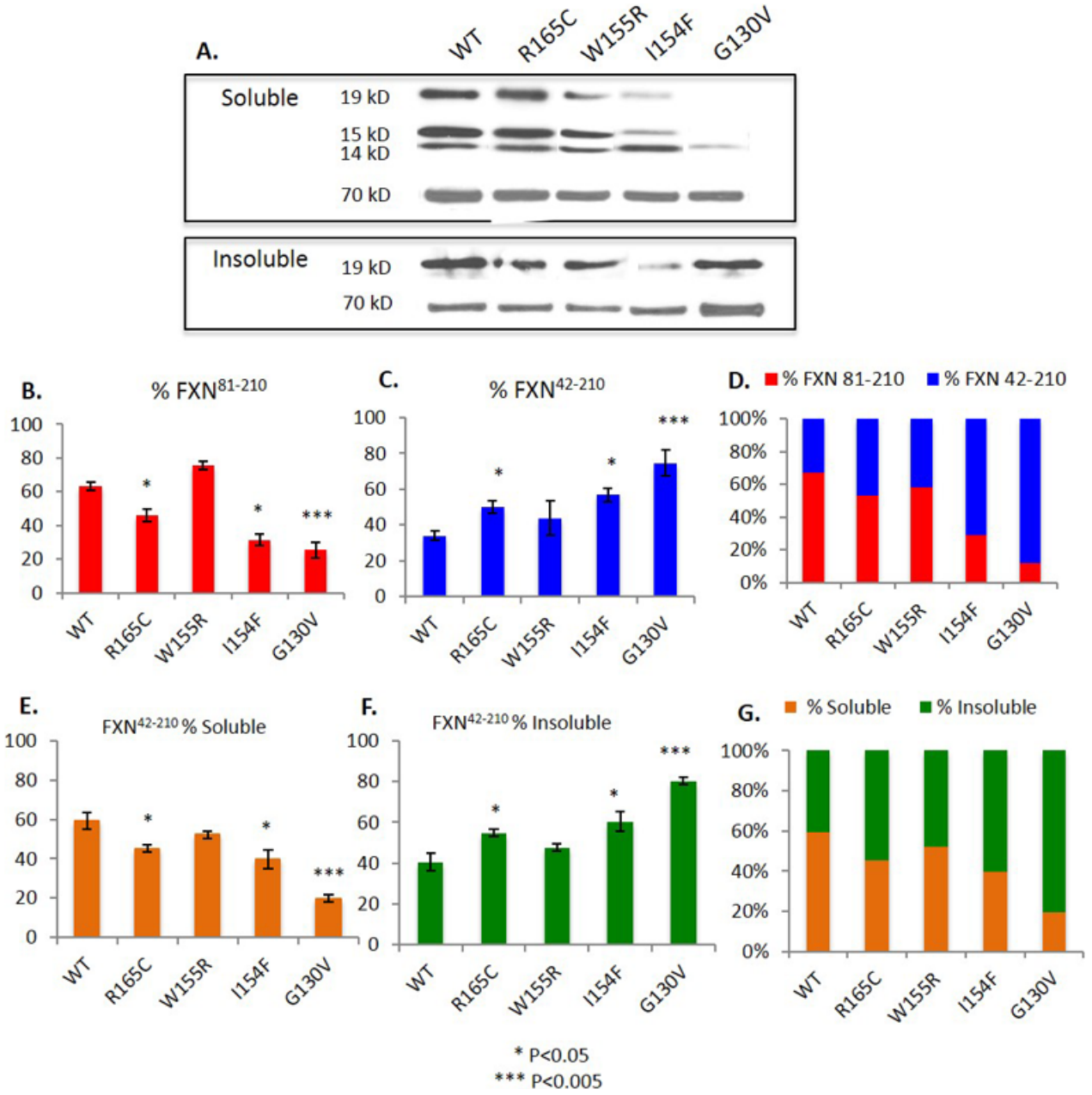

Figure 3. Selected FRDA-associated missense mutations impair processing from FXN^{42-210} to FXN^{81-210}. Following transfection of mutant constructs in HEK 293 cells, whole cell lysates were centrifuged to perform subcellular fractionation of soluble mitochondria fraction and insoluble mitochondrial pellet. **A.** FXN levels were detected by western blot using an anti-FXN antibody. Anti-SDHA antibody was used to detect SDHA as a mitochondria marker and loading control. The soluble mitochondria fraction includes: exogenous FXN^{42-210} (19 kD), exogenous FXN^{81-210} (15 kD), endogenous FXN^{81-210} (14 kD), and SDHA (70 kD). The insoluble mitochondria pellet includes: exogenous FXN^{42-210} (19 kD) and SDHA (70 kD). **B.** Percent FXN^{81-210} of total FXN. **C.** Percent $^{FXN42-210}$ of total FXN. **D.** Total FXN. **E.** Percent soluble FXN^{42-210}. **F.** Percent insoluble FXN^{42-210}. **G.** Total FXN^{42-210}. (*) = $P < 0.05$ and (***) = $P < 0.005$.

abnormalities that could be related to the altered processing observed in vitro. Heterozygous (HTZ subjects) FRDA patients, with a missense mutation on one FXN allele and GAA expansion on the other, and typical homozygous (HMZ subjects) FRDA patients, with GAA expansions on both FXN alleles, have different clinical profiles when examined in a large natural history study (Table 1). In addition, patients carrying G130V mutations have

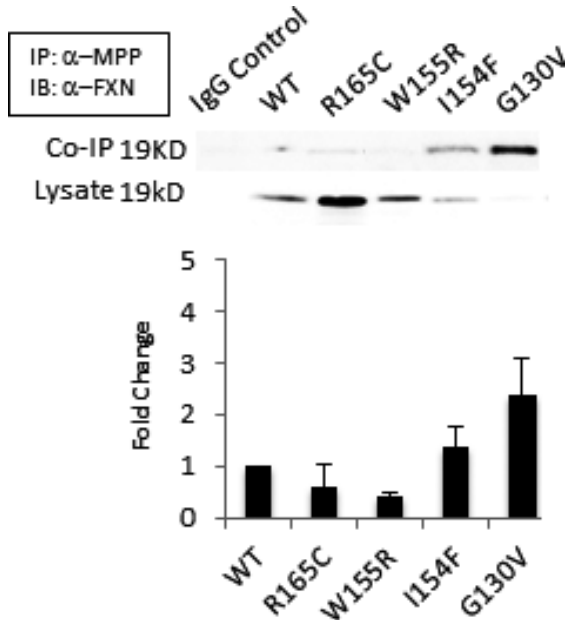

Figure 4. Missense mutations FXN^{I154F}and FXN^{G130V} enhance the association of FXN$^{42–210}$ with MPP. Whole cell lysates from transfected HEK 293 cells were immunoprecipitated with anti-MPP antibody and immunoblotted with primary anti-FXN antibody. The same whole cell lysates were used as inputs for quantification analysis. Western blot was used to detect FXN pulled down by anti-MPP. The Co-IP 19 kD blot represents immunoprecipitated FXN$^{42-210}$. The lysate 19 kD blot represents total FXN$^{42-210}$ in whole cell lysate. The graph represents fold change of FXN mutant interaction with MPP compared to FXN^{WT}.

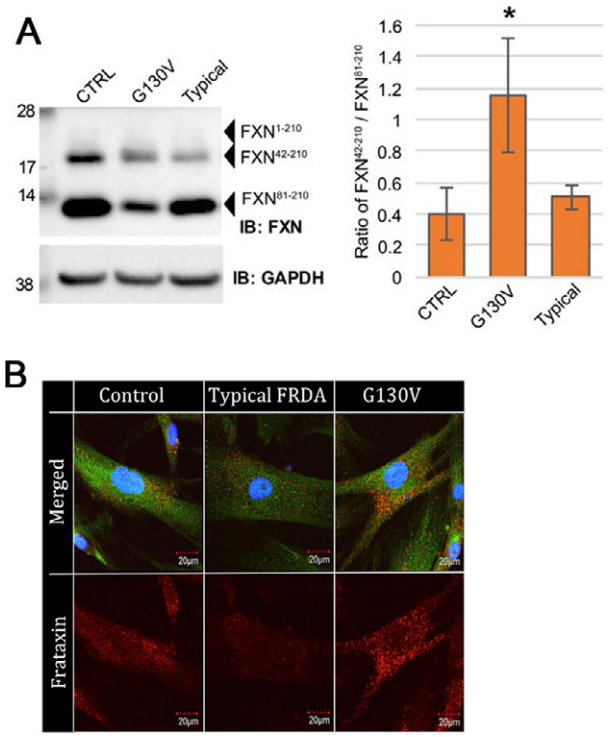

Figure 5. Increasing FXN^{G130V} and FXN^{I154F} FXN$^{1–210}$ levels does not increase FXN$^{81–210}$ levels. Following transfection of HEK 293 cells with mutant FXN constructs, cells were treated with 10 μmol/L MG132 proteasome inhibitor for 5 h followed by cell lysis. Exogenous FXN$^{1–210}$ (23 kD), FXN$^{42–210}$ (19 kD), and FXN$^{81–210}$ (15 kD) levels, before and after treatment, were detected by western blot using a primary anti-HA antibody.

significantly lower occurrence of cardiomyopathy, scoliosis, and diabetes, the most severe components of the disease, compared to other HTZ subjects (Table 1). Furthermore, clinical measures at baseline exam including ataxia stage, activities of daily living (ADL) scores, 9HPT-1, T25FW-1, Vision, 9HPT, Z2, and Z3 were significantly worse in other HTZ subjects, even though the groups were of similar disease duration, suggesting a less severe phenotype in G130V patients (Table 2). Patients with an I154F mutation fell between the phenotypic severity of G130V and other point mutations analyzed.

Discussion

This study shows that the FRDA-causing mutations FXN^{G130V} and FXN^{I154F} decrease FXN$^{81–210}$ levels, but do not impair FXN localization to mitochondria. FXN^{G130V} and FXN^{I154F} appear to impair FXN processing from FXN$^{42–210}$ to FXN$^{81–210}$, as well as enhance binding of FXN$^{42–210}$ to MPP. This impaired processing is also observed in primary fibroblasts from FRDA patients with a G130V mutation. Increasing FXN^{G130V} and FXN^{I154F} precursor levels does not lead to an increase in FXN$^{81–210}$ levels, but does increase levels of FXN$^{42–210}$. These are all consistent with a defect in peptide processing of these forms being a pathogenic mechanism in patients carrying these mutations. In addition, these two forms, especially G130V, are associated with milder features of FRDA than other point mutations or expanded GAA repeats, suggesting that these mild phenotypes may reflect the underlying FXN biochemistry.

In heterologous systems, disease-associated mutations in FXN are abnormal in several mutation selective ways. The inability to detect FXN^{L106S} and FXN^{G137V} by immunostaining and western blot supports modeling studies suggesting that mutations residing within the protein core decrease protein stability.[9] In vitro functional studies have also characterized FXN^{R165C} and FXN^{W155R} as dysfunctional mutations, causing decreased binding of FXN to Fe-S cluster assembly complex.[16,17] Moreover, FXN^{R165C} and FXN^{W155R} had levels of FXN$^{81–210}$ that were comparable to FXN^{WT}, and there was no evidence for impaired processing of these two mutant forms from FXN$^{42–210}$ to FXN$^{81–210}$. Further functional studies in vivo

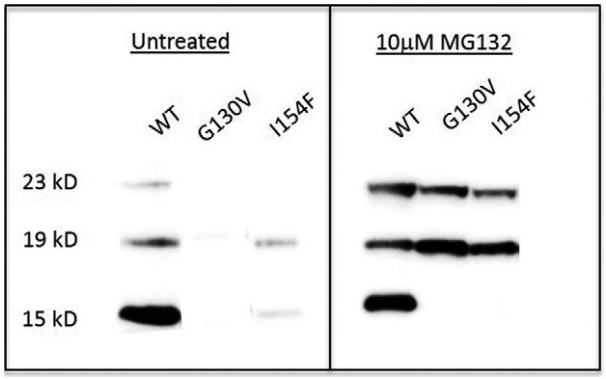

Figure 6. Impaired FXN processing from $FXN^{42–210}$ to $FXN^{81–210}$ occurs in fibroblasts from FRDA patients with FXN^{G130V}. FXN levels were quantified by western blot using whole cell extracts from control (CTRL), FRDA, and G130V patient fibroblasts. CTRL= 5 fibroblast lines (n = 13), G130V =3 lines (n = 17), and Typical = 7 lines (n = 8). **A.** $FXN^{42–210}$ (18 kD), and $FXN^{81–210}$ (13 kD) levels from control (CTRL), G130V, and typical FRDA were detected from whole cell extracts by western blot using an anti-FXN antibody. Detection of GAPDH serves as a loading control. FXN levels are quantified and expressed as a ratio of $FXN^{42–210}$ to $FXN^{81–210}$. (*) = $P < 0.05$. **B.** Confocal microscopy images of patient fibroblasts (CTRL, FRDA, and G130V) that were fixed and stained using primary anti-FXN and primary anti-mitofusin antibodies. Secondary antibodies included Alexa Fluor 568 (FXN) and Alexa Fluor 488 (mitofusin). DAPI was also used as a nuclear stain.

Table 1. Clinical measures comparing FRDA homozygous and heterozygous patients

	HMZ	HTZ
N	741 (96%)	32 (4%)
Age of Onset	13.8	10.7*
BL age	26.5	24
Recent age	30	27.3
Duration	16.2	16.6
Sex (%female)	49.40%	43.80%
Nonambulatory	50.20%	46.90%
Cardiomyopathy	57.80%	34.6%*
Scoliosis	82.40%	73.10%
Diabetes	5.50%	26.9%*
FARS	69.4	61.7
Stage	4	3.9
ADL	16.3	13.4
9HPT-1 (high = less severe)	0.014	0.025*
T25FW-1 (high = less severe)	0.055	0.062
Vision	105.3	100.6
Z2 (high = less severe)	−0.09	0.48*
Z3 (high = less severe)	−0.08	0.26

Patients who were heterozygous (HTZ) for the GAA repeat (those carrying point mutations or deletions) had similar disease durations to those who were homozygous (HMZ), but, aside from age of onset and presence of diabetes, were less severely affected than homozygous patients. This was particularly true for measures containing upper extremity function such as the nine-hole peg test and the Z2 score.

*$P < 0.05$.

may provide a correlation between the extent of dysfunction in these two FXN-mutant proteins and severity of disease outcome.

Abnormalities in FXN processing have been explored mostly in yeast and bacteria expression systems.[14,19–21] Here, we show an increased level of the $FXN^{42–210}$ form in disease-associated missense mutations associated with milder phenotypes, not only in overexpression studies using mammalian systems, but also in primary fibroblasts from FRDA patients. FRDA patients who carry G130V express lower $FXN^{81–210}$ levels than typical FRDA patients in fibroblasts, cheek swabs, and blood,[22] yet have a milder clinical phenotype (Tables 1 and 2). In a large cohort of FRDA subjects, even though those with the G130V mutation have similar disease duration, they have significantly better FARS and ADL scores than individuals with other point mutations. FRDA G130V patients also have significantly lower occurrence of cardiomyopathy, scoliosis, and diabetes, and they surpass other point mutation carrying subjects on composite performance measures. As suggested in single cases previously, this demonstrates that FRDA patients with FXN^{G130V} demonstrate greater neurological function and decreased disease severity at a similar length of disease duration.[8,10,11,15,23–29] Patients with I154F mutations have clinical severities intermediate between other patients with point mutations and G130V patients, matching the data from cellular models of the molecular consequences of these mutants.

One explanation for the milder phenotype in patients carrying a G130V or I154F mutation is that the incompletely processed $FXN^{42–210}$ carries some residual activity. In these mutants, this form is located in the mitochondria, and others suggest that $FXN^{42–210}$ can perform Fe-S cluster synthesis as well as participate in cysteine desulfurase activity as efficiently as $FXN^{81–210}$.[30,31] Thus, the higher levels of $FXN^{42–210}$ associated with FXN^{G130V} could lead to the mild phenotype of patients with G130V if this intermediate form is functional. Alternatively, it is possible that a small but clinically significant amount of the $FXN^{42–210}$ form is slowly converted to the mature form, leading to the milder phenotype in patients carrying G130V mutations compared with other mutations that yield absolutely no mature FXN. Further experiments examining the functional abilities of the $FXN^{42–210}$ form of endogenous FXN^{G130V} may help clarify these possibilities. Overall, the present study, in agreement with modeling studies and those in lower animal expression systems, identifies multiple mechanisms in mammalian

Table 2. Clinical measures comparing FXN^{G130V} and $FXNI^{154F}$ patients with other FRDA heterozygous patients

	G130V	I154F	Other HTZ
N	9	3	18
Age of Onset (years)	10.8	11	11.5
BL age (years)	21.4	22.6	11.5
Recent age (years)	23.4	25	23.5
Duration (years)	12.4	14	15.9
Sex (%female)	44	67	44
Cardiomyopathy (%)	12.5	0	50
Scoliosis (%)	50	100	78.6
Diabetes (%)	12.5	6.7	35.7
FARS	40.6	54.3	72.4
Stage	2.4	3.5	4.5
ADL	5.8	8	17.5
9HPT-1 (high = less severe)	0.044	0.029	0.015
T25FW-1 (high = less severe)	0.139	0.117	0.026
Vision	127.8	125.5	85.3
Z2 (high = less severe)	2.03	0.99	−0.21
Z3 (high = less severe)	1.55	0.79	−0.38

FRDA patients with FXN^{G130V} have milder disease features and slower disease progression compared to other heterozygous FRDA patients. Clinical data were collected from a large natural history study of FRDA, including data on medical history, genetic status, disability and activity of daily living (ADL) status, a quantitative neurological exam (designated the Friedreich ataxia rating scale [FARS]), performance measures, and two performance measure composites. When we fractionated the heterozygous patients into patients those carrying G130V versus I154F versus others, the G130V patients were markedly less affected. I154F patients had levels of dysfunction between G130V and other heterozygous patients.

heterologous systems by which FXN point mutations can lead to FRDA.

Acknowledgments

This work was supported in part by the NIH training program in neuropsychopharmacology at the University of Pennsylvania (R01MH109260), as well as by grants from the NIH (R21NS**0**87343) and (R01NS081366 to MN) and the Friedreich Ataxia Research alliance to DRL, MN, and JSB. We also acknowledge the Collaborative Clinical Research Network in Friedreich Ataxia for their contribution to the clinical data.

Author Contribution

EC, JSB, IC, MN, and DRL conceived and designed the study. EC, JSB, and CI acquired and analyzed the data.

Conflict of Interest

None declared.

References

1. Bidichandani S, Delatycki M. Friedreich Ataxia. Gene Reviews 2014.
2. Marmolino D. Friederich's ataxia: past, present, and future. Brains Res Rev J 2011;2:311–330.
3. Campuzano V, Montermini L, Dolores Molto M, et al. Friedreich's ataxia: autosomal recessive disease caused by an lntronic GAA triplet repeat expansion. Science 1996;271:1423–1427.
4. Gonzalez-Cabo P, Vazquez-Manrique V, Adelaida Garcia-Gimeno M, et al. Frataxin interacts functionally with mitochondrial electron transport chain proteins. Hum Mol Genet 2005;14:2091–2098.
5. Dürr A, Cossee M, Agid Y, et al. Clinical and genetic abnormalities in patients with Friedreich's ataxia. N Engl J Med 1996;335:1169–1175.
6. Filla A, De Michele G, Cavalcanti F, et al. The relationship between trinucleotide (GAA) repeat length and clinical features in Friedreich ataxia. Am J Hum Genet 1996;59:554–560.
7. Montermini L, Richter A, Morgan K, et al. Phenotypic variability in Friedreich ataxia: role of the associated GAA triplet repeat expansion. Ann Neurol 1997;41:675–682.
8. Forrest S, Knight M, Delatycki M, et al. The correlation of clinical phenotype in Friedreich ataxia with the site of point mutations in the FRDA gene. Neurogenetics 1998;1:253–257.
9. Galea CA, Huq A, Lockhart PJ, et al. Compound heterozygous FXN mutations and clinical outcome in Friedreich ataxia. Ann Neurol 2016;79:485–495.
10. McCormack ML, Guttmann RP, Schumann M, et al. Frataxin point mutations in two patients with Friedreich's ataxia and unusual clinical features. J Neurol Neurosurg Psychiatry 2000;68:661–664.
11. Cossée M, Dürr A, Schmitt M, et al. Friedreich's ataxia: point mutations and clinical presentation of compound heterozygotes. Ann Neurol 1999;45:200–206.
12. Santos R, Lefevre S, Sliwa D, et al. Friedreich Ataxia: molecular mechanisms, redox considerations, and therapeutic opportunities. Antioxid Redox Signal 2010;13:651–690.
13. Dhe-Pananon S, Shigeta R, Chi YI, et al. Crystal structure of human frataxin. J Biol Chem 2000;275:30753–30756.
14. Cavadini P, Gellera C, Patel P, et al. Human frataxin maintains mitochondrial iron homeostasis in *Saccharomyces cerevisiae*. Hum Mol Genet 2000;9:2523–2530.
15. Bidichandani S, Ashizawa T, Patel P. Atypical Friedreich ataxia caused by compound heterozygosity for a novel missense mutation and the GAA triplet-repeat expansion. Am J Hum Genet 1997;60:1251–1256.
16. Bridwell-Rabb J, Winn AM. Barondeau DP structure-function analysis of Friedreich's ataxia mutants reveals determinants of frataxin binding and activation of the Fe-S assembly complex. Biochemistry 2011;50:7265–7274.

17. Tsai C, Bridwell-Rabb J, Barondeau DP. Friedreich's ataxia variants I154F and W155R diminish frataxin-based activation of the iron-sulfur cluster assembly complex. Biochemistry 2011;50:6478–6487.
18. Patel M, Isaacs C, Seyer L, et al. Progression of Friedrich ataxia: quantitative characterization over five years. Ann Clin Transl Neurol 2016;3:684–694.
19. Koutnikova H, Campuzano V, Koenig M. Maturation of wild-type and mutated frataxin by the mitochondrial processing peptidase. Hum Mol Genet 1998;7:1485–1489.
20. Gordon D, Shi Q, Dancis A, et al. Maturation of frataxin within mammalian and yeast mitochondria: one-step processing by matrix processing peptidase. Hum Mol Genet 1999;8:2255–2262.
21. Cavadini P, Adamec J, Taroni F, et al. Two-step processing of human frataxin by mitochondrial processing peptidase. J Biol Chem 2000;52:41469–41474.
22. Lazaropulos M, Dong Y, Clark E, et al. Measurement of frataxin levels in peripheral tissue in Friedreich ataxia: analysis using repeated measures. Ann Clin Transl Neurol 2015;8:831–842.
23. Delatycki M, Williamson R, Forrest S. Friedreich ataxia: an overview. J Med Genet 2000;37:1–8.
24. Parkinson MH, Boesch S, Nachbauer W, et al. Clinical features of Friedreich's ataxia: classical and atypical phenotypes. J Neurochem 2013;1:103–117.
25. Gellera C, Castellotti B, Mariotti C, et al. Frataxin gene point mutations in Italian Friedreich ataxia patients. Neurogenetics 2007;8:289–299.
26. Zühlke CH, Dalski A, Habeck M, et al. Extension of the mutation spectrum in Friedreich's ataxia: detection of an exon deletion and novel missense mutations. Eur J Hum Genet 2004;12:979–982.
27. McCabe DJ, Wood NW, Ryan F, et al. Intrafamilial phenotypic variability in Friedreich ataxia associated with a G130V mutation in the FRDA gene. Arch Neurol 2002;59:296–300.
28. Delatycki MB, Knight M, Koenig M, et al. G130V, a common FRDA point mutation, appears to have arisen from a common founder. Hum Genet 1999;105:343–346.
29. Calmels N, Schmucker S, Wattenhofer-Donzé M, et al. The first cellular models based on frataxin missense mutations that reproduce spontaneously the defects associated with Friedreich ataxia. PLoS ONE 2009;4:e6379.
30. Vaubel RA, Isaya G. Iron-sulfur cluster synthesis, iron homeostasis and oxidative stress in Friedreich ataxia. Mol Cell Neurosci 2013;55:50–61.
31. Li H, Gakh O, Smith DY, et al. Missense mutations linked to Friedreich ataxia have different but synergistic effects on mitochondrial frataxin isoforms. J Biol Chem 2013;6:4116–4127.

